Electrocatalytic Reduction of CO_2 at Au Nanoparticle Electrodes: Effects of Interfacial Chemistry on Reduction Behavior

Evan Andrews,[a,*] Sai Katla,[b] Challa Kumar,[b] Matthew Patterson,[c] Phillip Sprunger,[c] and John Flake[a,,z]**

[a]*Gordon and Mary Cain Department of Chemical Engineering, Louisiana State University, Baton Rouge, Louisiana 70803, USA*
[b]*Center for Advanced Microstructures and Devices, Louisiana State University, Baton Rouge, Louisiana 70806, USA*
[c]*Department of Physics & Astronomy, Louisiana State University, Baton Rouge, Louisiana 70803-4001, USA*

Nanoscale Au electrocatalysts demonstrate the extraordinary ability to reduce CO_2 at low overpotentials with high selectivity to CO. Here, we investigate the role of surface chemistry on CO_2 reduction behavior using Au_{25} and 5 nm Au nanoparticles. Onset potentials for CO_2 reduction at Au_{25} nanoparticles in Nafion binders are shifted anodically by 190 mV while the hydrogen evolution reaction is shifted cathodically by 300 mV relative to Au foil. The net effect of this beneficial separation in onset potentials is relatively high Faradayic efficiencies for CO (90% at 0.8 V versus RHE) at high current densities. Experimental results show Faradayic efficiencies for CO are greatest using electrodes made with Nafion-immobilized Au_{25} nanoparticles. Likewise, CO_2 reduction onset potential shifts are greater for smaller nanoparticles and when Nafion binders are used instead of (sulfonate-free) polyvinylidene fluoride. X-ray photoelectron spectroscopy analysis reveals Au nanoparticles may react with the sulfonates of Nafion binders. The results suggest sulfonate interfaces may alter the binding energies of key species or lead to favorable reconstructions, either of which ultimately results in remarkable improvements in Faradayic efficiencies relative to Au foil electrodes.
© The Author(s) 2015. Published by ECS. This is an open access article distributed under the terms of the Creative Commons Attribution 4.0 License (CC BY, http://creativecommons.org/licenses/by/4.0/), which permits unrestricted reuse of the work in any medium, provided the original work is properly cited. [DOI: 10.1149/2.0541512jes] All rights reserved.

Manuscript submitted July 16, 2015; revised manuscript received August 26, 2015. Published September 12, 2015. This was Paper 1523 presented at the Chicago, Illinois, Meeting of the Society, May 24–28, 2015.

The electrochemical reduction of CO_2 holds promise to generate energy-dense fuels using only atmospheric CO_2, water and solar or wind energy. In recent works, several types of wet-synthesized metal nanoclusters (Au, Ag, Pt, Pd, Cu) have been demonstrated in electrochemical sensors[1–3] or electrolytic cells[3–5] with remarkable advantages over conventional metal (foil) electrodes. Recent works using Au_{25} nanoclusters as electrochemical sensors demonstrate nanomolar sensitivity for species such as dopamine, ascorbic acid, uric acid, iodide or nitrites.[6–8] Likewise composite electrodes with Au, Ag and Cu nanoclusters have shown desirable current-potential behaviors in CO_2 and O_2 reduction reactions including significantly lower onset potentials relative to their foil analogs (>100 mV). The underlying nature of activity enhancements associated with the structure or surface chemistry of composite nanocluster electrodes is not well established. As with enzymatic mechanisms, it is possible that structural effects associated with the ligated surface may facilitate specific reactant or product interactions. It is also possible that both kinetic and thermodynamic benefits originate from unique properties associated with under-coordinated (or ligated) metal atoms that result in improved binding energies or reduced transition state energies. In general, literature reports suggest decreasing particle dimensions increases catalytic activity;[9,10] however, trends in the electrochemical behavior associated with adsorbed ligands are less clear.[11,12] Recent work by Liu et al.[13] shows alkyl-terminated Pt nanoparticles (2.85 nm) exhibit semiconducting behavior while phenyl-terminated Pt nanoparticles of the same size demonstrate metallic behavior and are more active in the oxygen reduction reaction (ORR). Another work focusing on the ORR using Ag nanoparticles[11] showed phenyl-terminated Ag nanoparticles resulted in a ∼200 mV anodic shift in onset potentials versus bare nanoparticles, while thiol-capped Ag nanoparticles resulted in a ∼160 mV cathodic shift. The authors attributed the improved ORR behavior of phenyl-terminated Ag nanoclusters to an electronic structure that results in improved oxygen adsorption. As with enzymes, adsorbed ligands may also influence the behavior of electrodes through both passive (e.g. selective adsorption)[14,15] or active mechanisms (e.g. improved binding).[16,17] Here we investigate the electrochemical reduction of CO_2 at Au surfaces including Au_{25} and 5 nm nanoparticles with thiol or citrate terminations and consider the role of polyvinylidene fluoride (PVDF) and Nafion binders in composite electrodes.

The well-known Turkevich[18–20] and Brust-Schiffrin[21–24] synthesis methods are particularly useful for producing solutions of ligand-stabilized Au, Ag or Cu nanoclusters (<10 nm) using reducing agents and stabilizers.[25–29] The Turkevich method typically yields nanoclusters with citrate capping ligands and the conventional Brust-Schiffrin preparation method results in nanoclusters with thiol ligands. While thiols readily to bind to Au, Ag and Cu surfaces; several other S-containing ligands including benzenesulfonates,[30] disulfides,[31] trithiolates,[32] thioacetates,[33] and dithiocarbamates[34] have also been used to stabilize Au nanoparticles. In contrast with gas phase heterogeneous catalysis where sulfur species are generally considered poisons, these thiol-protected Au nanoclusters are particularly interesting candidates as electrocatalysts,[35,36] especially considering their unique electronic states resembling molecules rather than a metals.[3,37] For example, Jin et al. recently demonstrated Au_{25} nanoclusters in CO_2 reduction with reduction onset potentials at −0.193 V vs RHE (Relative Hydrogen Electrode) which is approximately 200 mV positive of the onset potential for the same reaction at Au foil electrodes.[38,39] The authors attributed the improvement in performance to the promotion of CO_2 adsorption due to unique associations between the Au_{25} and CO_2. The ability to leverage ligand and size effects to lower CO_2 reduction onset potentials can have profound effects due to the exponential relationship between current and potential (e.g. Butler-Volmer kinetics). Thus, the efficiency and selectivity (or Faradayic efficiencies) to form fuels such as CO or CH_4 from CO_2 may be drastically improved since the desired reduction reaction occurs significantly positive of the hydrogen evolution reaction (HER).[40–42]

While the structure and surface chemistry of Au nanoclusters has been well characterized, it is possible that surfaces may be altered in the electrode preparation process or in the CO_2 reduction process itself (this is particularly true for composite electrodes with polymer binders). Conventional Au_{25} nanoclusters synthesized using phenylethylthiol ligands are typically anionic for some time after synthesis though they eventually destabilize into a neutral form.[43,44] In the case of Au_{25}, the Au atoms are structured in a core-shell configuration, where an icosahedral Au_{13} core is surrounded by an outer shell of 12 additional Au atoms and 18 thiol ligands.[43,45] As shown in Figure 1, the S atoms in the outer shell form bidentate bonds with Au atoms in

*Electrochemical Society Student Member.
**Electrochemical Society Active Member.
[z]E-mail: johnflake@lsu.edu

Downloaded on 2018-06-11 to IP 192.107.175.1 address. Redistribution subject to ECS terms of use (see ecsdl.org/site/terms_use) unless CC License in place (see abstract).

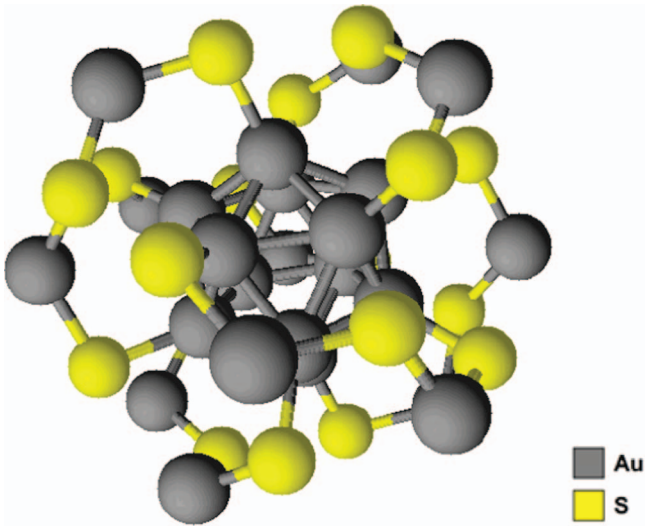

Figure 1. Structure of thiol-protected Au_{25} nanoclusters. The structure consists of an icosahedral 13 Au atom core and a 12 Au atom outer shell.

the outer shell. These twenty-five atom nanoclusters are considered the most stable due to the bidentate thiolates.[46] It is also important to note that the particular thiolate may be exchanged for another ligand.[47] Some thiol ligands may be reduced at potentials positive of the CO_2 reduction reaction; however, longer-chain or aromatic thiols are more stable and may remain adsorbed at Au surfaces at the potentials used for CO_2 reduction. In fact, recent SFG (Sum Frequency Generation) spectroscopy work by Baldelli et al.[48] shows that longer chain thiols remain near the surface even after their reduction. In addition to the ligand interface associated with nanoparticle synthesis, it is also important to understand the effect of the binder. In practice, a binder should be inert and support well-dispersed nanoparticles within a conductive matrix while allowing the transport of reactants and products (similar to the role of binders in battery electrodes). In this work, we focus on fluoropolymer binders such as PVDF and Nafion. Nafion is a well-known proton-conducting sulfonated fluoropolymer, commonly used in nanoparticle inks. The binders are similar; however, Nafion's sulfonate moieties facilitate proton transfer within the porous film. While reactions between Au species and these fluoropolymers are not expected, it is important to note that that sulfonates may chemisorb to Au surfaces.[49,50] In the case with thiolated Au_{25} nanoclusters, the thiolated surfaces are expected to be relatively stable in with either binder since thiol monolayers on Au films are stable across a wide range of pH values.[51]

In this work, we consider citrate and thiolate terminations of Au nanoclusters along with porous Nafion and PVDF (sulfonate-free) binders. We investigate the gas and liquid products of aqueous electrochemical CO_2 reduction using Au_{25} nanoclusters as a function of binder and surface chemistry. Voltammetry is used to characterize the electrochemical behavior and nanoparticles were studied using UV-visible spectroscopy and XPS (X-ray Photoelectron Spectroscopy). Altogether, these studies reveal fascinating current voltage and yield behavior as a function of Au nanoparticle size and surface chemistry.

Experimental

Au_{25} nanoclusters were prepared using established methods[52] and integrated into conductive inks for subsequent use as electrodes. In the synthesis process, phenyl thiol-stabilized $[Au_{25}(SCH_2CH_2Ph)_{18}]^-$ clusters were made by solvating tetrachloroaurate(III) trihydrate (0.4 mmol $HAuCl_4.3H_2O$) in ultra-pure DI water and phase-transferring to toluene with tetraoctyl ammonium bromide (0.47 mmol TOAB). The aqueous layer was then decanted and the toluene solution containing the Au salt was purged with N_2 and cooled to 0°C. Phenylethylthiol (0.17 mL $PhCH_2CH_2SH$) was added as a capping agent. The reduction was performed at 0°C by adding sodium borohydride (4 mmol $NaBH_4$) in ultra-pure water at 0°C. The aqueous layer was decanted and the toluene solution was dried. Ethanol was added to separate Au_{25} clusters from TOAB and other side products. The Au_{25} clusters were collected after removing the supernatant and purified by extracting twice with acetonitrile (MeCN).

The 5 nm thiol-capped Au nanoclusters were made using other established methods[53] and also integrated into conductive inks. In this synthesis procedure, $HAuCl_4.3H_2O$ (0.25 mmol) was solvated in DI water and phase transferred into toluene via TOAB. The aqueous layer was then decanted and dodecanethiol added as a capping agent. The reduction was performed at 55°C using a tert butyl-amine borane complex (Sigma Aldrich). The toluene solution was evaporated and ethanol added to separate the 5 nm Au clusters from TOAB and other side products. The remaining nanoparticles were again dispersed in acetone. Other 5 nm Au nanoparticles with citrate termination were obtained commercially from BBInternational for use in spectroscopy studies.

Nanoparticle electrodes were made by depositing composite inks onto glassy carbon electrodes. The Au_{25}/Nafion and Au 5 nm/Nafion inks were prepared by mixing Vulcan XC-72R carbon black (100 mg), 5% Nafion (1.2 mL) (Sigma Aldrich), and ~10 mg of Au nanoparticles solvated in acetone (1 mL). Likewise, Au_{25}/PVDF and Au 5 nm/PVDF inks were prepared by mixing Vulcan XC-72R carbon black (100 mg), 5% PVDF solvated in N-methyl-pyrrolidone (1.2 mL) (Sigma Aldrich), and ~10 mg of Au nanoparticles solvated in acetone (1 mL). In this case, electrodes were synthesized using approximately 5 mL of citrate colloid solution (0.316 mg Au) mixed with 0.5 mL Nafion and 40 mg of carbon black. All ink mixtures were sonicated for 30 minutes before application to electrode surfaces. Inks were applied to 5 mm diameter glassy carbon electrodes in a Teflon sheath (Pine Instruments) using a brush and allowed to dry at room temperature for approximately 24 hours.

Nanoparticles surfaces and solutions of nanoparticles were examined using XPS and UV-visible spectroscopy. Substrates specifically intended for XPS analyses were prepared in the same fashion using 1 cm^2 polished glassy carbon (STI) or Ag(111) single crystals. Au_{25} samples including: Au_{25} in toluene, Au_{25} in acetone with 0.05% by weight Nafion and Au_{25} in acetone with 0.05%wt PVDF before and after use in CO_2 reduction reactions were deposited dropwise onto the surface and allowed to dry. Citrate-terminated Au colloid samples including 5 nm Au in water and 5 nm Au in water with 0.05%wt Nafion were prepared similarly. The samples were mounted onto Ta sample holders using graphite tape for transfer into the XPS system. All XPS experiments were performed in an ultra-high vacuum chamber with base pressure of 1×10^{-10} Torr. Measurements were performed using an Omicron XM1000 source providing monochromatic Al $K\alpha_1$ radiation ($h\nu = 1486.6$ eV) and a Specs PHOIBOS 150 hemispherical analyzer. High-resolution spectra of the Au 4f region were recorded using 20 eV pass energy. Sample charging was not observed in any XPS spectra, as verified using the C 1s line from the glassy carbon substrate. Spectra were de-convoluted using the fitting routines available in CasaXPS.

UV-visible absorption characteristics of nanoparticle solutions were obtained using a Hitachi U-2001 NIR-UV-VIS Spectrophotometer in acetone (including solvent spectra subtraction). The Au_{25} nanoclusters samples were freshly synthesized followed by the addition of 0.5%wt Nafion or 0.5%wt PVDF in n-methyl pyrrolidone (NMP). The same samples without Au_{25} were also prepared to ensure other solvents or binders did not interfere with the Au_{25} absorption peaks. Absorption spectra were recorded between 300 and 900 nm wavelengths.

Aqueous electrochemical experiments were conducted in a two-compartment cell with a Nafion membrane as described in a previous work.[54] The catholyte was continuously bubbled with CO_2, and the vent led directly to a GC auto-injection port. A Pt wire was used as the counter electrode in the anolyte with an Ag/AgCl reference electrode. The saturated CO_2 solution included 0.1M $KHCO_3$ (Sigma Aldrich) and was operated at room temperature (22°C). The pH of carbonate

Downloaded on 2018-06-11 to IP 192.107.175.1 address. Redistribution subject to ECS terms of use (see ecsdl.org/site/terms_use) unless CC License in place (see abstract).

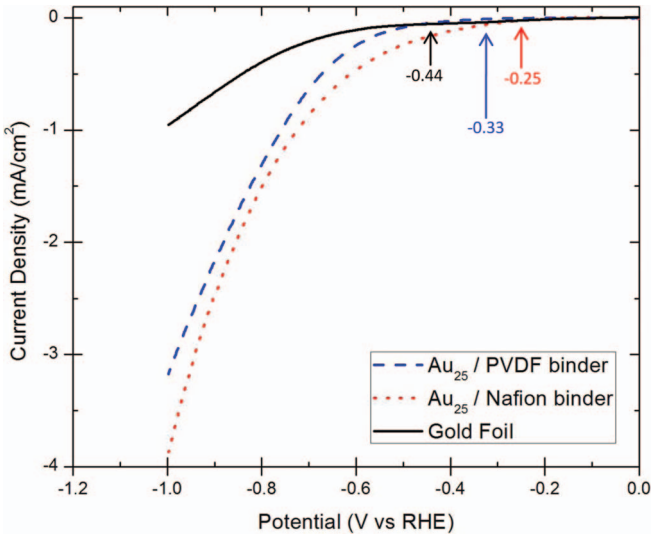

Figure 2. Linear voltammograms of gold foil, Au_{25}/Nafion and Au_{25}/PVDF in CO_2 saturated 0.1M $KHCO_3$.

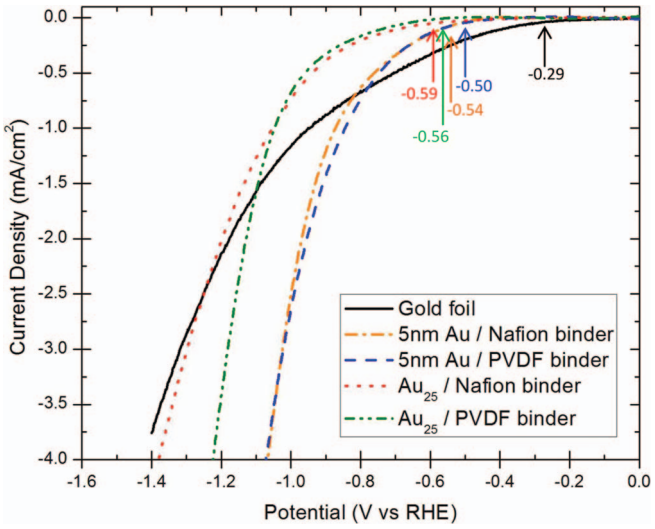

Figure 4. Linear voltammograms of gold foil, Au_{25}/Nafion, Au_{25}/PVDF, 5 nm Au/Nafion and 5 nm Au/PVDF in nitrogen purged 0.1 M $KHCO_3$.

electrolyte was measured at 6.8 when saturated with CO_2, and 8.9 when purged with N_2. These values were used when converting to the RHE scale. Voltammetry was conducted at a scan rate of 10 mV/s. Reaction yields were determined using potentiostatic experiments using gas chromatography (GC) (TCD & FID) or nuclear magnetic resonance spectroscopy (NMR) to analyze gas and liquid products (with a reaction time of at least 1h). Liquid samples were taken before and after each reaction and analyzed using NMR spectroscopy (Varian System 700, 5 mm HCN probe) using methods previously reported.[41,54]

Results and Discussion

Linear sweep voltammetry was used to study the current density and onset potentials of the CO_2 reduction reaction at several electrodes: Au foil, 5 nm Au nanoclusters and Au_{25} nanoclusters in both Nafion and PVDF binders. Onset potentials were determined by plotting the log of the current versus potential followed by linear extrapolation. As shown in Figures 2 and 3, the onset potentials for CO_2 reduction is dependent on both the size of the nanocluster and binder. At Au_{25}/PVDF electrodes, the CO_2 reduction onset is shifted anodically by 70 mV relative to Au foil while the CO_2 reduction onset potential with Au_{25}/Nafion electrodes is shifted anodically by 190 mV relative to Au foil. Likewise, on 5 nm Au/PVDF electrodes the onset is shifted anodically by 60 mV relative to Au foil, while on 5 nm Au/Nafion electrodes the onset is shifted anodically by 140 mV relative to Au foil (Figure 3). Onset potentials for CO_2 reduction at Au foil (near −0.44 V versus the RHE) and the shift observed with Au/Nafion electrodes are consistent with previous works;[38,39,55] however, the effect of the binder (Nafion versus PVDF) is striking. Reduction current-potential behavior and current densities are similar in each case; note the current associated with composite electrodes is normalized by the geometric area of the glassy carbon.

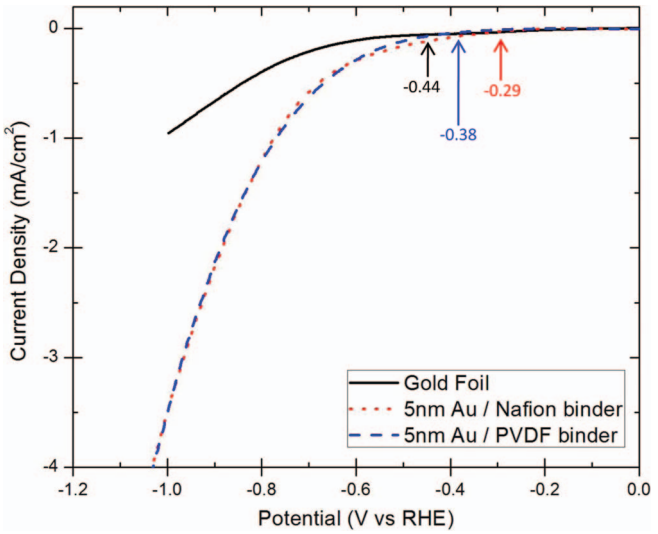

Figure 3. Linear voltammograms of gold foil, 5 nm Au/Nafion and 5 nm Au/PVDF in CO_2 saturated 0.1 M $KHCO_3$.

The onset potential of the hydrogen evolution reaction (HER) in the absence of CO_2 was also studied using linear sweep voltammetry. As shown in Figure 4, the HER onset potential is shifted cathodically for both Au_{25} (300 mV in Nafion, 280 mV in PVDF) and 5 nm Au nanoparticles (250 mV in Nafion, 210 mV in PVDF) relative to Au foil.

The combined anodic shifts for CO_2 reduction and cathodic shifts for the HER are extremely beneficial for CO production in terms of both selectivity and yield. It is important to note that even relatively small shifts separating the onset potentials for CO reduction and HER can result profound improvements on the practical ability to generate fuels due to the exponential current - overpotential relationship. The results can be seen in the improved Faradayic efficiencies for CO production at lower overpotentials and relatively high current densities. As shown in Figures 5 and 6, the primary products of the reduction reaction were determined to be CO and H_2 along with trace amounts of formate (<1% Faradayic efficiency). The Faradayic efficiency of CO for Au_{25} clusters in the Nafion binder increased with cathodic potential, up to ∼90% Faradayic efficiency at −0.8 V versus RHE. At the same potential, Au_{25} clusters in PVDF binder reached CO Faradayic efficiencies near 55% while the larger 5 nm Au nanoparticles electrodes reached a maximum near 41% when using a Nafion binder. For comparison, these Faradayic efficiencies are significantly greater than those than for bulk gold at similar potentials (FE∼4.6% at −0.8 V).[39]

A key question centers on the nature of the improvement to the CO_2 reduction and HER onset potentials. Previous studies suggest that the improvement may be due to the contributions of both the reduction site and surface chemistry of the nanoclusters. The anodic shift of CO_2 reduction is may be due to reduced CO binding energy at the low-coordinated active sites on the gold nanoclusters, as suggested by Peterson and Nørskov.[56–59] In fact, a recent work by

Downloaded on 2018-06-11 to IP 192.107.175.1 address. Redistribution subject to ECS terms of use (see ecsdl.org/site/terms_use) unless CC License in place (see abstract).

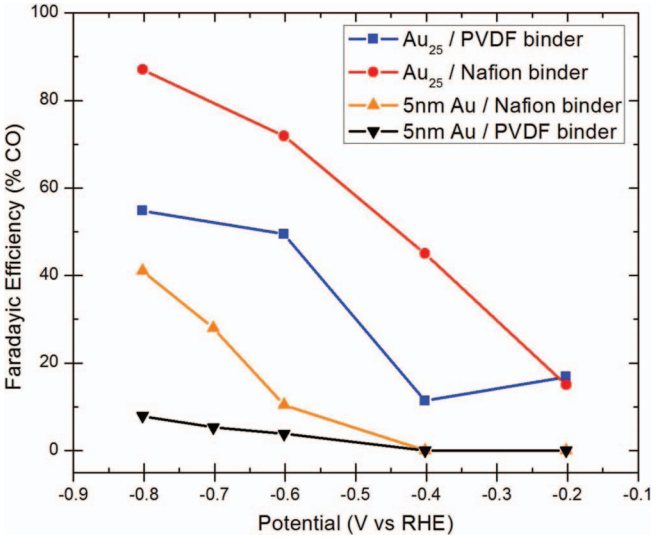

Figure 5. Faradayic efficiency plot for CO production of Au_{25}/Nafion, Au_{25}/PVDF, 5 nm Au/Nafion and 5 nm Au/PVDF catalyst inks.

Peterson et al.[60] demonstrates that CO generation is favored at the edge sites of Au nanowires while the HER is favored at corner sites, so nanowires with relatively high edge to corner ratios improve CO_2 reduction and suppress the HER. Further, another work by Peterson et al. suggests that local environment (particularly oxides at Cu surfaces) can also influence CO_2 reduction selectivity.[61] In the case of Au with thiolated surfaces, work by Jin et al. considers the unique interactions between CO_2 and Au_{25} (weakly bound) due to charge redistributions in the thiolated-Au_{25} clusters as the key mechanism responsible for improved CO_2 reduction behavior. In addition to promoting CO_2 reduction, it is also possible that the ligands may interfere with hydrogen formation. Adsorbed thiols are known to result in cathodic shifts in the onset potential for the HER on Au surfaces[62] and the results from this study (Figure 4) also show cathodic shifts in HER onset potentials for all thiolated nanoparticle electrodes relative to Au foil. In this case, the most dramatic differences in reduction behavior are the anodic shifts in CO_2 reduction associated with the binder (viz. Nafion).

The voltammetric behavior and Faradayic efficiencies observed with Au_{25} or 5 nm Au nanoparticle electrodes suggest that the sulfonate moieties of Nafion contribute to shifts in onset potentials. In the case of Au_{25} nanoparticles, the differences in onset potentials between the CO_2 reduction and HER were ~340 mV with Nafion versus ~220 mV with PVDF. The larger window (between CO_2 onset and HER onset) associated with Nafion could be related to reactions between the thiolated Au_{25} nanoparticles and sulfonate groups of the Nafion binder. Previous work by Negishi et al. suggests that sulfates can oxidize Au_{25}, causing the formation of stable $[Au_{25}(SCH_2CH_2Ph)_{18}]^+$ species;[46] however, these species should be easily reduced at the potentials used for CO_2 reduction. It is also possible that the equilibrium associated with the bidentate thiols is shifted by the relatively high concentration of sulfonates, leading to an exchange of thiolates for sulfonates.

XPS was used to study the oxidation state of the Au in the nanoparticles. Figure 6 shows XPS spectra from three Au_{25} samples: 1. "as prepared" (bottom), 2. mixed with binders before the reaction (middle), and 3. the same electrodes after their use in CO_2 reduction for 15 minutes at −1.4 V vs Ag/AgCl (top). The Au 4f peaks show the expected 3.7 eV split due to spin-orbit interactions, but both are shifted approximately 0.8 eV to higher binding energy compared to bulk Au. This shift is comparable to results previously found for Au_{25} nanoparticles synthesized through different methods, and has been attributed to initial-state effects due to the small particle size.[63] The Au 4f peaks for the Au_{25}/Nafion ink electrode (left side of Figure 6) shows the same set of peaks as the Au_{25} reference, but also shows two new shoulders with higher binding energies, including a smaller spin-orbit split (3.5 eV vs. 3.7 eV for the reference spectrum) associated with partially oxidized Au_{25} clusters. The majority of the spectra

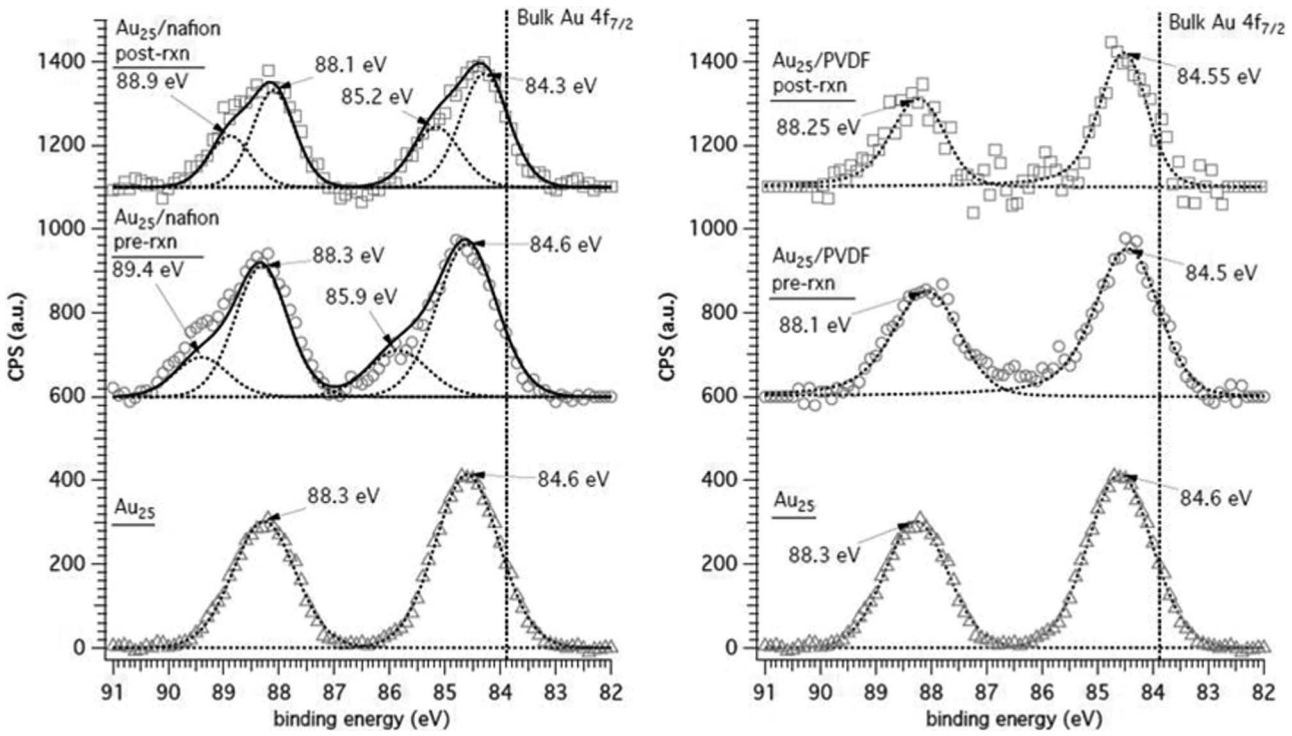

Figure 6. Au 4f XPS spectra. On the left, from bottom to top, Au_{25} nanoparticles in toluene deposited on an Ag single-crystal substrate, an Au/Nafion sample on glassy carbon prior to reaction, and an Au/Nafion sample on glassy carbon after reaction. On the right, from bottom to top, Au_{25} nanoparticles in toluene deposited on an Ag single-crystal substrate, an Au/PVDF sample on glassy carbon prior to reaction, and an Au/PVDF sample on glassy carbon after reaction. The vertical dotted lines indicate the binding energy of bulk gold.

Downloaded on 2018-06-11 to IP 192.107.175.1 address. Redistribution subject to ECS terms of use (see ecsdl.org/site/terms_use) unless CC License in place (see abstract).

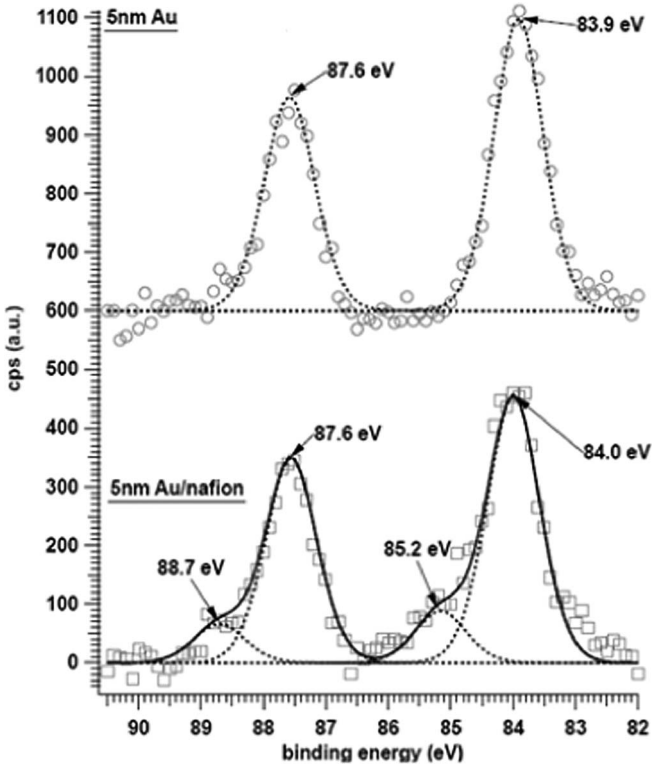

Figure 7. Au 4f XPS spectra. The top spectra shows 5 nm citrate protected Au colloid sample on glassy carbon. The bottom spectra shows a 5 nm citrate protected Au colloid sample with a dilute Nafion binder on glassy carbon.

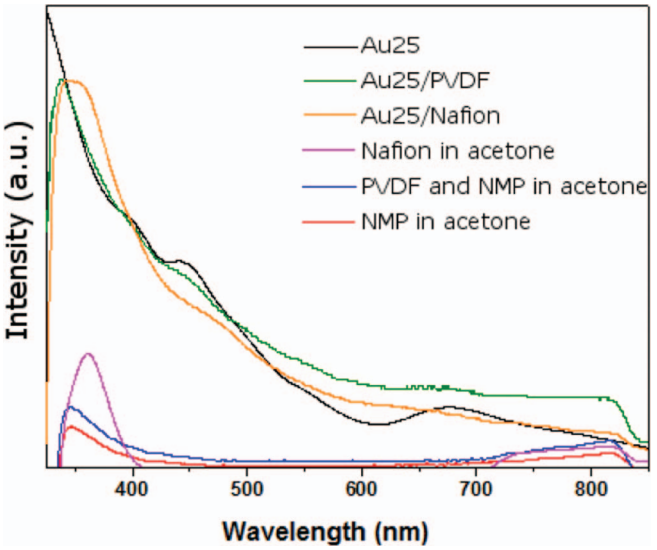

Figure 8. UV-visible data showing the spectra for freshly synthesized Au_{25} nanoclusters in acetone, Au_{25} in acetone with dilute PVDF dissolved in NMP and Au_{25} in acetone with dilute Nafion as well as control spectra for Nafion, NMP and PVDF in acetone. Peaks at ~400, 450, and 670 indicate thiol bridged Au_{25} clusters and are visible in the PVDF and fresh Au_{25} samples, but not in the dilute Nafion sample.

remains identical to those fit to the Au_{25} reference sample and suggests that core Au atoms may remain intact. These results suggest the equilibrium associated with high concentrations of sulfonates in the Au_{25}/Nafion system may lead to sulfonated Au interfaces. After the CO_2 reduction reaction, the shoulders remain; suggesting the new Au_{25} species in the Nafion binder may be relatively stable or is easily re-formed after the reduction reaction. The small peak shift observed between 0.2–0.7 eV after the reaction may be associated with partial desorption at cathodic potentials; however, this is not considered significant. As shown in Figure 7, another XPS analysis using 5 nm Au nanoparticles made with either citrate or thiolate capping ligands show the same secondary peaks associated with sulfonated Au species arising when combined with Nafion. In the case with the larger 5 nm Au nanoparticles, the relative area of the secondary peaks is somewhat smaller, consistent with the lower surface-to-volume ratio of the larger nanoparticles. Here it is important to note that ligand exchange (sulfonate for thiolate) in itself does not necessarily change the oxidation state of the Au;[47] however, it may be possible that sulfonates destabilize the initial bridge sulfur atom in the outer shell of Au_{25} resulting in a partially oxidized surface. This may result in relatively lower CO binding energies or it is also possible that the surfaces of the nanoparticles are reconstructed into relatively more active sites for CO_2 reduction.

UV-visible spectroscopy was used to evaluate to the structure of Au nanoparticles, shown in Figure 8. In the spectra for Au_{25} nanoclusters (in acetone), there are absorption peaks at ~400, 450, and 670 nm which are indicative of the Au_{25} structure, detailed in previous reports.[64,65] A second spectra taken after the addition of PVDF to the Au_{25} solution indicates Au_{25} nanoclusters retain a similar structure even after exposure to PVDF. The peak strength is lower due to dilution; however, peak locations are otherwise unchanged. In contrast, after the addition of Nafion to the Au_{25} solution, the peaks at 400 and 670 nm are lost, and the 450 nm peak is shifted to a higher wavelength suggesting either an agglomeration or alteration of the nanoparticle. While it is possible that some Au_{25} particles may agglomerate in the liquid phase used for UV-visible spectroscopy, the Au_{25} spectra in PVDF and the spectra in Nafion remained constant over several hours and did not resemble the spectra associated with the larger 5 nm Au particles. This behavior along with the voltammetry, yields and XPS analyses suggests that the particles likely remain as 25 atom clusters albeit with an altered structure.

The underlying nature of the improved Faradayic efficiency for CO generation may be associated with both the size and surface chemistry of the Au nanoparticles. As noted previously, the sulfonate interaction is somewhat unexpected, since the thiolates are generally considered to be relatively stable especially with magic-number nanoclusters.[46,66,67] However, it is possible the relatively high concentrations of sulfonate species may shift the equilibrium to favor sulfonated Au_{25} interfaces; and it is also possible that these interfaces favor CO generation and/or prevent the HER. The enhanced CO_2 reduction observed with Nafion binders was observed using both 5 nm Au and Au_{25} nanoparticles suggesting that the primary origin of the decreased CO_2 onset potentials is likely associated with sulfonate interactions rather than the size or anionic charge associated with Au_{25}. While the surface chemistry and preferential reduction sites remain unknown under reduction conditions, it is possible that sulfonated interfaces change the binding energies of adsorbed CO_2, CO or other intermediates similar to the role of copper oxides.[61] In this case, a more weakly bound CO species (in the presence of sulfonated interfaces) could result in the anodic shift observed in CO_2 reduction onset potentials. Another potential origin for the improvements in reduction behavior may be due to reconstruction of Au surfaces caused by the exposure to sulfonates. The reconstruction (similar to the oxygen-induced restructuring of Au surfaces observed by Friend et al.)[71] could provide sites that are relatively more active to CO_2 reduction. This effect would be particularly important in the case of Au_{25} where the loss of the bidentate ligands could lead to a longer more rod-like structure.[72] As noted by Peterson et al, edge sites associated with nanorods are particularly valuable to improve the reduction selectivity to CO.[60] In either case, there is considerable evidence that the Au surface chemistry plays a strong role in CO_2 reduction behavior and that these interface effects may be leveraged to improve selectivity and/or Faradayic efficiencies.

Downloaded on 2018-06-11 to IP 192.107.175.1 address. Redistribution subject to ECS terms of use (see ecsdl.org/site/terms_use) unless CC License in place (see abstract).

Conclusions

The close proximity of the formal potentials for the electrochemical generation of CO and H_2 form a fundamental barrier to the efficient production of fuels from CO_2. Here, we demonstrate nanoscale Au electrocatalysts and interfaces that are particularly useful in promoting CO_2 reduction while preventing the HER. As shown in linear sweep voltammetry and Faradayic efficiencies, Au nanoclusters immobilized in Nafion are significantly more active at reducing CO_2 to CO than the same Au nanoclusters immobilized in PVDF binders or Au foil. The sulfonate environment appears to provide a ∼170 mV anodic shift in the onset for CO_2 reduction with Au_{25} nanoparticles and a ∼140 mV shift in the onset with 5 nm Au nanoparticles versus Au foil, whereas are the shifts are only 70 mV and 60 mV (respectively) for the same nanoparticles in PVDF binders. The results indicate that interfacial chemistry plays a substantial (perhaps dominant) role in determining reduction selectivity relative to the size or charge of the nanoparticles. Based on these results, the underlying mechanism for the improved Faradayic efficiencies for CO production may be attributed changes in the binding energies induced by the Au-sulfonate surface or favorable reconstructions in the presence of sulfonates (or a combination of these effects).

Acknowledgments

This work was supported by the Center for Atomic Level Catalyst Design, an Energy Frontier Research Center funded by the U.S. Department of Energy, Office of Science and the Office of Basic Energy Sciences under Award Number DE-SC0001058 as well as the National Science Foundation under grant CBET-1438385,

References

1. J. Macanás, M. Farre, M. Muñoz, S. Alegret, and D. N. Muraviev, *physica status solidi (a)*, **203**(6), 1194 (2006).
2. L.-H. Li and W.-D. Zhang, *Microchim Acta*, **163**(3-4), 305 (2008).
3. S. Guo and E. Wang, *Nano Today*, **6**(3), 240 (2011).
4. Z. Liu, X. Y. Ling, X. Su, and J. Y. Lee, *The Journal of Physical Chemistry B*, **108**(24), 8234 (2004).
5. B. Fang, N. K. Chaudhari, M.-S. Kim, J. H. Kim, and J.-S. Yu, *Journal of the American Chemical Society*, **131**(42), 15330 (2009).
6. S. S. Kumar, K. Kwak, and D. Lee, *Analytical chemistry*, **83**(9), 3244 (2011).
7. G. Baek, P. Pandurangan, E. Ko, Y. Mo, and D. Lee, *RSC Advances*, **4**(21), 10766 (2014).
8. K. Kwak, S. S. Kumar, and D. Lee, *Nanoscale*, **4**(14), 4240 (2012).
9. M. Nesselberger, S. Ashton, J. C. Meier, I. Katsounaros, K. J. J. Mayrhofer, and M. Arenz, *Journal of the American Chemical Society*, **133**(43), 17428 (2011).
10. K. Bergamaski, A. L. N. Pinheiro, E. Teixeira-Neto, and F. C. Nart, *The Journal of Physical Chemistry B*, **110**(39), 19271 (2006).
11. G. Q. He, Y. Song, B. Phebus, K. Liu, C. P. Deming, P. G. Hu, and S. W. Chen, *Science of Advanced Materials*, **5**(11), 1727 (2013).
12. Y. J. Tong, (1460 (Electronic)).
13. K. Liu, X. Kang, Z.-Y. Zhou, Y. Song, L. J. Lee, D. Tian, and S. Chen, *Journal of Electroanalytical Chemistry*, **688**(0), 143 (2013).
14. T. Moffat, B. Baker, D. Wheeler, and D. Josell, *Electrochemical and solid-state letters*, **6**(4), C59 (2003).
15. N. Hai, T. Huynh, A. Fluegel, M. Arnold, D. Mayer, W. Reckien, T. Bredow, and P. Broekmann, *Electrochimica Acta*, **70** 286 (2012).
16. G. K. Jennings and P. E. Laibinis, *Journal of the American Chemical Society*, **119**(22), 5208 (1997).
17. T. Diemant, J. Bansmann, and H. Rauscher, *ChemPhysChem*, **11**(7), 1482 (2010).
18. J. Turkevich, P. C. Stevenson, and J. Hillier, *Discussions of the Faraday Society*, **11**(0), 55 (1951).
19. S. S. Shankar, S. Bhargava, and M. Sastry, *Journal of nanoscience and nanotechnology*, **5**(10), 1721 (2005).
20. K. Zabetakis, W. E. Ghann, S. Kumar, and M.-C. Daniel, *Gold Bulletin*, **45**(4), 203 (2012).
21. M. Brust, M. Walker, D. Bethell, D. J. Schiffrin, and R. Whyman, *Journal of the Chemical Society, Chemical Communications*, (7), 801 (1994).
22. M. Brust, M. Walker, D. Bethell, D. J. Schiffrin, and R. Whyman, *J. Chem. Soc., Chem. Commun.*, (7), 801 (1994).
23. P. J. Goulet and R. B. Lennox, *Journal of the American Chemical Society*, **132**(28), 9582 (2010).
24. M. Brust, J. Fink, D. Bethell, D. Schiffrin, and C. Kiely, *J. Chem. Soc., Chem. Commun.*, (16), 1655 (1995).
25. P. Zhao, N. Li, and D. Astruc, *Coordination Chemistry Reviews*, **257**(3–4), 638 (2013).
26. K. Tan and K. Cheong, *J Nanopart Res*, **15**(4), 1 (2013).
27. T. Udayabhaskararao and T. Pradeep, *The Journal of Physical Chemistry Letters*, **4**(9), 1553 (2013).
28. P. Zhao, N. Li, and D. Astruc, *Coordination Chemistry Reviews*, **257**(3), 638 (2013).
29. D. Seo and H. Song, *Gold Nanoparticles for Physics, Chemistry and Biology*, 103 (2012).
30. S. Wang, K. Qian, X. Bi, and W. Huang, *The Journal of Physical Chemistry C*, **113**(16), 6505 (2009).
31. Y. Li, O. Zaluzhna, and Y. J. Tong, *Chemical Communications*, **47**(21), 6033 (2011).
32. K. Wojczykowski, K. Mei, P. Jutzi, I. Ennen, A. Hutten, M. Fricke, and D. Volkmer, *Chemical Communications*, (35), 3693 (2006).
33. S. Zhang, G. Leem, and T. R. Lee, *Langmuir*, **25**(24), 13855 (2009).
34. S. Sung, H. Holmes, L. Wainwright, A. Toscani, G. J. Stasiuk, A. J. P. White, J. D. Bell, and J. D. E. T. Wilton-Ely, *Inorganic Chemistry*, **53**(4), 1989 (2014).
35. M.-C. Daniel and D. Astruc, *Chemical Reviews*, **104**(1), 293 (2003).
36. R. Sardar, A. M. Funston, P. Mulvaney, and R. W. Murray, *Langmuir*, **25**(24), 13840 (2009).
37. R. Jin, *Nanoscale*, **2**(3), 343 (2010).
38. Y. Hori, in *Modern Aspects of Electrochemistry*, C. Vayenas, R. White, and M. Gamboa-Aldeco, eds., Vol. **42**, p. 89, Springer New York, (2008).
39. D. R. Kauffman, D. Alfonso, C. Matranga, H. Qian, and R. Jin, *Journal of the American Chemical Society*, **134**(24), 10237 (2012).
40. Y. Hori, A. Murata, K. Kikuchi, and S. Suzuki, *Journal of the Chemical Society, Chemical Communications*, (10), 728 (1987).
41. K. P. Kuhl, E. R. Cave, D. N. Abram, and T. F. Jaramillo, *Energy & Environmental Science*, **5**(5), 7050 (2012).
42. Y. Hori, A. Murata, and R. Takahashi, *Journal of the Chemical Society, Faraday Transactions 1: Physical Chemistry in Condensed Phases*, **85**(8), 2309 (1989).
43. M. W. Heaven, A. Dass, P. S. White, K. M. Holt, and R. W. Murray, *Journal of the American Chemical Society*, **130**(12), 3754 (2008).
44. M. Zhu, C. M. Aikens, F. J. Hollander, G. C. Schatz, and R. Jin, *Journal of the American Chemical Society*, **130**(18), 5883 (2008).
45. J. Akola, M. Walter, R. L. Whetten, H. Häkkinen, and H. Grönbeck, *Journal of the American Chemical Society*, **130**(12), 3756 (2008).
46. Y. Negishi, N. K. Chaki, Y. Shichibu, R. L. Whetten, and T. Tsukuda, *Journal of the American Chemical Society*, **129**(37), 11322 (2007).
47. E. S. Shibu, M. A. H. Muhammed, T. Tsukuda, and T. Pradeep, *The Journal of Physical Chemistry C*, **112**(32), 12168 (2008).
48. J. D. C. Jacob, T. R. Lee, and S. Baldelli, *The Journal of Physical Chemistry C*, **118**(50), 29126 (2014).
49. R. L. Garrell, J. E. Chadwick, D. L. Severance, N. A. McDonald, and D. C. Myles, *Journal of the American Chemical Society*, **117**(46), 11563 (1995).
50. K. Kreuer, M. Ise, A. Fuchs, and J. Maier, *J. Phys. IV France*, **10**(PR7), Pr7-279–Pr277-281 (2000).
51. B.-K. Kong, Yong-Seong Choi, and S. Insung, *Bulletin of the Korean Chemical Society*, **29**(9), 4 (2008).
52. M. Zhu, E. Lanni, N. Garg, M. E. Bier, and R. Jin, *Journal of the American Chemical Society*, **130**(4), 1138 (2008).
53. N. Zheng, J. Fan, and G. D. Stucky, *Journal of the American Chemical Society*, **128**(20), 6550 (2006).
54. E. Andrews, M. Ren, F. Wang, Z. Zhang, P. Sprunger, R. Kurtz, and J. Flake, *Journal of The Electrochemical Society*, **160**(11), H841 (2013).
55. Y. Hori, A. Murata, K. Kikuchi, and S. Suzuki, *J. Chem. Soc., Chem. Commun.*, (10), 728 (1987).
56. A. A. Peterson, F. Abild-Pedersen, F. Studt, J. Rossmeisl, and J. K. Nørskov, *Energy & Environmental Science*, **3**(9), 1311 (2010).
57. J. Kleis, J. Greeley, N. A. Romero, V. A. Morozov, H. Falsig, A. H. Larsen, J. Lu, J. J. Mortensen, M. Dułak, K. S. Thygesen, J. K. Nørskov, and K. W. Jacobsen, *Catalysis Letters*, **141**(8), 1067 (2011).
58. M. Mavrikakis, P. Stoltze, and J. K. Nørskov, *Catalysis Letters*, **64**(2-4), 101 (2000).
59. A. Sanchez, S. Abbet, U. Heiz, W. D. Schneider, H. Häkkinen, R. N. Barnett, and U. Landman, *The Journal of Physical Chemistry A*, **103**(48), 9573 (1999).
60. W. Zhu, Y.-J. Zhang, H. Zhang, H. Lv, Q. Li, R. Michalsky, A. A. Peterson, and S. Sun, *Journal of the American Chemical Society*, **136**(46), 16132 (2014).
61. Y.-J. Zhang and A. A. Peterson, *Physical Chemistry Chemical Physics*, **17**(6), 4505 (2015).
62. H. Hagenström, M. A. Schneeweiss, and D. M. Kolb, *Langmuir*, **15**(7), 2435 (1999).
63. G. A. Simms, J. D. Padmos, and P. Zhang, *The Journal of Chemical Physics*, **131**(21), 214703 (2009).
64. M. Zhu, W. T. Eckenhoff, T. Pintauer, and R. Jin, *The Journal of Physical Chemistry C*, **112**(37), 14221 (2008).
65. J. C. Yang, H. Xu, S. Gao, L. Menard, L.-L. Wang, A. Frenkel, D. Johnson, and R. Nuzzo, *Microscopy and Microanalysis*, **11**(SupplementS02), 1548 (2005).
66. H. Sellers, A. Ulman, Y. Shnidman, and J. E. Eilers, *Journal of the American Chemical Society*, **115**(21), 9389 (1993).
67. W. Kurashige, Y. Niihori, S. Sharma, and Y. Negishi, *The Journal of Physical Chemistry Letters*, **5**(23), 4134 (2014).
68. X. Wu, L. Senapati, S. K. Nayak, A. Selloni, and M. Hajaligol, *The Journal of Chemical Physics*, **117**(8), 4010 (2002).
69. M. J. Hynes and J. A. Maurer, *Molecular BioSystems*, **9**(4), 559 (2013).
70. C. G. Worley and R. W. Linton, *Journal of Vacuum Science & Technology A*, **13**(4), 2281 (1995).
71. B. K. Min, X. Deng, D. Pinnaduwage, R. Schalek, and C. M. Friend, *Physical Review B*, **72**(12), 121410 (2005).
72. T. Iwasa and K. Nobusada, *The Journal of Physical Chemistry C*, **111**(1), 45 (2007).

Downloaded on 2018-06-11 to IP 192.107.175.1 address. Redistribution subject to ECS terms of use (see ecsdl.org/site/terms_use) unless CC License in place (see abstract).